Direct Probing of Oxygen Loss from the Surface Lattice of Correlated Oxides during Hydrogen Spillover

Hyojin Yoon[1], Yongjin Kim[2, 3], Ethan J. Crumlin[4], Donghwa Lee[1, 2], Kyuwook Ihm[3,#] and Junwoo Son[1,*]

[1]Department of Materials Science and Engineering, Pohang University of Science and Technology (POSTECH), Pohang 37673, Republic of Korea.

[2]Division of Advanced Material and Science, Pohang University of Science and Technology (POSTECH), Pohang 37673, Republic of Korea

[3]Nano & Interface research Team, Pohang Accelerator Laboratory, Pohang 37673, Republic of Korea

[4]Advanced Light Source, Lawrence Berkeley National Laboratory, Berkeley, California 94720, USA

Abstract

Hydrogen spillover is a catalytic process that occurs by surface reaction and subsequent diffusion to reversibly provide a massive amount of hydrogen dopants in correlated oxides, but the mechanism and surface chemistry at the surface of correlated oxides with metal catalyst are not well understood. Here we show that a significant amount of oxygen is released from the surface of correlated VO_2 films during hydrogen spillover, contrary to the well-established observation of the formation of hydrogen interstitials in the bulk part of VO_2 films. By using ambient-pressure X-ray photoelectron spectroscopy, we prove that the formation of surface oxygen vacancies is a consequence of a favorable reaction for the generation of weakly-adsorbed H_2O from surface O atoms that have low coordination and weak binding strength. Our results reveal the importance of *in-situ* characterization to prove the dynamic change during redox reaction, and presents opportunity to control intrinsic defects at the surface.

Keywords: correlated oxide; hydrogen spillover; surface oxygen vacancy; bulk hydrogen interstitial; in-situ characterization

[#] johnet97@postech.ac.kr, [*] jwson@postech.ac.kr

Hydrogen spillover is a result of the exceptional catalytic activity of noble metals with hydrogen gas (H_2); the process has been utilized for possible applications as a method to store hydrogen in solid materials under near-ambient conditions [1-7]. In combinations of a catalytic metal and a transition-metal oxide support (e.g., Pt/WO_3, Pt/MoO_3, Au/TiO_2), the noble metal surface provides sites to break the H-H bond[1, 4-6, 8]; In this process, the H_2 first undergoes dissociative chemisorption upon interacting with noble metal catalysts, then atomic H is spilled over onto the oxide support that contacts the metal catalyst. For example, in Pt-decorated MoO_3 support, the resulting atomic H migrate from the Pt surface into the reducible MoO_3 support. Then a massive number of atomic H diffuse throughout the bulk support with hydrogen spillover at low temperature by forming blue conducting H_xMoO_3 in the oxide support [1, 6, 9].

This principle has potential use as a method to supply hydrogen atoms in correlated oxides that undergo metal-insulator transition (e.g., VO_2, $SmNiO_3$, $NdNiO_3$) to reversibly modulate electronic phase by filling electrons provided by hydrogens[10-15]. This process suppresses formation of oxygen vacancies owing to low-temperature annealing assisted by Pt catalyst, and thereby maintaining the crystal framework in correlated oxides. The incorporated hydrogen forms O-H bonds in the lattice, which cause electrons occupation in the conduction *d* band (t_{2g} or e_g band) of correlated materials. Up to one hydrogen per chemical unit can be incorporated by hydrogen spillover into VO_2 lattices without any loss of oxygen.[10] This hydrogen spillover process allows us to elucidate two-step phase modulation from insulator (VO_2, $3d^1$) to metal (H_xVO_2; $0 < x < 1$) to insulator (HVO_2, $3d^2$) during inter-integer *d*-band filling of electrons[10, 13]. Likewise, metal-insulator transition controlled by band filling has also been demonstrated using hydrogen

spillover in RNiO$_3$ (R = rare earth), which are also correlated materials that have e_g^1 electron configuration [11, 12, 16].

Suppression of the oxygen vacancy formation causes incorporated hydrogens to be located in the interstitial sites in bulk lattice of correlated oxides during hydrogen spillover [10, 11, 14, 15], but the surface chemistry of correlated oxides during the process remain unknown. The phenomenon of hydrogen spillover is related to surface reactions and subsequent diffusion, so to fully understand the processes, the adsorbed intermediates and surface chemistry must be characterized *in situ* at the surface of correlated oxide with metal catalyst.[1, 6] *In situ* crystal and electronic structure modulation in bulk correlated materials during hydrogen spillover has been previously quantified using X-ray diffraction (XRD) and X-ray absorption spectroscopy (XAS) at the ambient condition[10, 13, 15, 17, 18], but real-time monitoring of the surface with H_2 gas has not been performed using X-ray photoelectron spectroscopy (XPS) since XPS could be typically characterized under ultra-high vacuum due to too short inelastic mean free path of photoelectrons in the presence of gas.

Here, we use synchrotron-based *in situ* ambient pressure X-ray photoelectron spectroscopy (APXPS) to investigate the mechanism of the modulation in vanadium and oxygen surface chemistry of VO_2 epitaxial films during hydrogen spillover. During the spillover, the binding energy of the vanadium core level gradually decreased while the binding energy of the oxygen core level increased; these concurrent trends confirm that vanadium valence states are reduced at the surface. Quantitative analysis of each deconvoluted photoelectron spectra peak as a function of time showed direct evidence of oxygen loss at the surface of correlated VO_2 films

during the catalytic process: A significant amount of oxygen was released from the lattice (i.e., the formation of surface oxygen vacancies) by forming adsorbed water molecules with weak binding during hydrogen spillover process. This is the first observation of the process, which is distinct from the dominant reaction of the formation of hydrogen-related defects (i.e., interstitials) in the bulk part of VO_2 films. The appearance of oxygen-related defects at the surface is attributed to the low coordination of surface atoms, which are energetically-favorable reaction sites for the generation of weakly-adsorbed water during hydrogen spillover.

The 10-nm-thick $(100)_R$-oriented VO_2 epitaxial films were grown on (0001) Al_2O_3 substrate by pulsed laser deposition as described elsewhere.[10] To achieve sufficient hydrogenation in the VO_2 films by using hydrogen spillover, nano-sized Pt islands were formed on the film surface as H_2 dissociation catalyst (**Fig. 1a**); this method effectively cracks H_2 molecules into H atoms by lowering the energy barrier to the surface reaction (i.e., adsorption and dissociation) of hydrogen molecules with VO_2 [10, 11, 13-15]. Then, out-of-plane lattice parameters of VO_2 films were characterized by *in situ* symmetrical XRD during hydrogen spillover at 70 °C to identify dynamic structural modulation of the entire thickness (~ 10 nm) in VO_2 films (**Fig. 1b**). Before hydrogenation, the peak of pristine VO_2 was located at ~2.785 $Å^{-1}$ with clear Kiessig fringes. During hydrogen spillover, the peak position shifted left to ~2.732 $Å^{-1}$ within 30 min, its peak intensity decreased by an order of magnitude, and its Kiessig fringes disappeared; these changes indicate small out-of-plane lattice expansion with the loss of uniform lattice modulation, and are similar to those studied in VO_2 films that are doped with a small amount of hydrogen [19]. In the end, the first peak completely disappeared and a new peak gradually saturated at 2.551 $Å^{-1}$ with

clear Kiessig fringes; these changes indicate huge out-of-plane lattice expansion by massive hydrogen uptake, and uniform distribution of hydrogen interstitials in the VO_2 lattices. Similar changes have been observed in VO_2 films during full hydrogenation [10, 13, 15, 20]. Thus, this Pt-catalyst-assisted low temperature process allowed giant lattice expansion along the out-of-plane direction; the process is a result of selective injection of hydrogen atoms into interstitial sites in the VO_2 lattice by suppressing oxygen vacancy formation. The penetrating and escaping depth of X-ray source and signal in XRD are much greater than the thickness of VO_2 films (~ 10 nm), so the giant expansion and contraction of the X-ray diffraction peak indicates that hydrogen uptake and release occurs in the entire layer of VO_2 film.

To directly confirm selective hydrogen incorporation in the VO_2 epitaxial film during hydrogen spillover at low temperature, the chemical compositions were compared before (**Fig. 1c**) and after (**Fig. 1d**) hydrogen spillover (50 °C, P_{H_2} = 5 mTorr for 8 h) by using negative ion depth profiles of time-of-flight secondary ion mass spectrometry (ToF-SIMS). The intensity of the selected ions (VO_2^-, Al^-, $^{18}O^-$ and H^-) with sputtering time indicates the compositional profile along the thickness direction of the films. The variation of VO_2^- and Al^- profiles defines the boundaries between VO_2 thin films and Al_2O_3 substrates. The intensity of H^- signals was almost the same in VO_2 films as in Al_2O_3 substrate before hydrogen spillover, which suggests that pristine VO_2 films contain background levels of hydrogens (**Fig. 1c**). After hydrogen spillover, the intensity of H^- in the VO_2 films increased by an order of magnitude above the background signal of H^-, but the intensity of VO_2^-, Al^-, $^{18}O^-$ did not change noticeably (**Fig. 1d**); this result validates that only hydrogen atoms migrated between oxygen atoms along the facile diffusion pathway.

This process causes valence reduction on the V atoms with the negligible loss in oxygen (i.e., topotactic phase transformation) in the entire VO_2 film, despite the reducing atmosphere.[10, 14, 15]

To monitor change in chemical bonding near the surface in real time, *in situ* APXPS was performed during hydrogen spillover of VO_2 thin films. First, to remove possible surface contaminants before hydrogen spillover, the samples were cleaned by heating at 250 °C in 100 mTorr O_2 [21, 22]; the cleanliness of the surface was confirmed by the complete disappearance of the contaminant-related C 1s peak, and the concurrent increase in the peak intensity of V 2p and O 1s (**Fig. S1**). Peak deconvolution of each spectrum from surface-treated sample revealed that the peak of O 1s consisted mostly of lattice oxygen (O-V) with negligible contribution from hydroxyl (O-H) (**Fig. S1d**), and that V^{4+} and V^{5+} coexisted on the surface after oxygen treatment after carbon removal [23, 24]. However, no peak related to V_2O_5 occurred in XRD after oxygen treatment; i.e., V^{5+} valence states form only at the surface, whereas VO_2 phase with V^{4+} valence state is maintained in the bulk of the films. This result indicates that VO_2 surfaces is over-oxidized with respect to stoichiometric composition after the exposure of O_2 gas; this conclusion is consistent with a previous prediction that used first principles calculation [25]: due to the presence of adsorbed oxygens in a wide range of thermodynamic conditions, the VO_2 surface tends to become over-oxidized by forming vanadyl (V=O) species rather than to be stoichiometric. Moreover, oxygen adsorption from the gas phase is strongly exothermic, so surface oxidation is thermodynamically favorable; this process leads to the natural formation of V^{5+} states at the surface.[23, 24]

Then, to characterize the dynamic modulation of surface states in contaminant-free clean Pt/VO_2 films under the H_2 pressure of 5 mTorr during hydrogen spillover, the V 2p and the O 1s spectra were acquired using APXPS at 670 eV photon energy with inelastic mean free paths in the range of 0.8 ~ 1.2 nm[26] (**Fig. 2**). The high X-ray monochromatic flux from synchrotron photon sources and differentially-pumped analyzers fitted with a small aperture cone in APXPS allow acquisition of good photoemission signals by minimizing the inelastic loss that occurs in the presence of gas (**Fig. 1a**).[27] Before spillover, the binding energy of V $2p_{3/2}$ and O 1s were located at ~ 517 eV and 530 eV, respectively. After H_2 gas had been introduced at 50 °C, the peak of the V $2p_{3/2}$ spectra decreased in intensity and gradually shifted toward lower binding energy, which results in peak broadening (**Fig. 2a**). Concurrently, the O 1s peak shifted toward higher binding energy with development of an additional peak shoulder (**Fig. 2b**). Although the change of Pt 4f is relatively negligible compared to the change of V 2p and O 1s, the spectra show the slight shift to the higher binding energy after hydrogen spillover, which might be attributed to the formation of Pt-H_{ads} or Pt^{δ}-OH_{ads} with higher binding energy than Pt^0 (**Fig. S3**).[28] The change of the V 2p and the O 1s spectra was fully reversible even after hydrogenation and dehydrogenation cycles, which excludes the effect of beam damage (**Fig. S4**)

For quantitative analysis, each spectrum was deconvoluted using Lorentzian-Gaussian (L-G) curves after background subtraction (**Fig. 2c**)[29]. The VO_2 surface was over-oxidized, so before hydrogen spillover, the V 2p spectra could be assigned to V^{4+} ($2p_{3/2}$, E_b ~ 515.84 eV, $2p_{1/2}$, E_b ~ 523.17 eV) and V^{5+} ($2p_{3/2}$, E_b ~ 517.2 eV, $2p_{1/2}$, E_b ~ 524.53 eV). During hydrogen spillover, the intensity of the deconvoluted V^{3+} peak ($2p_{3/2}$, E_b ~ 515.29 eV, $2p_{1/2}$, E_b ~ 522.62 eV) gradually

increased at the expense of V^{4+} and V^{5+} peaks (**Fig. 2c**); this change is a result of the reduction of vanadium valence states. In case of O 1s spectra, initial quantitative deconvolution fitted the O 1s peak perfectly using two peaks, which correspond to a dominant contribution from lattice oxygen (O-V, E_b ~ 530 eV) and a relatively small contribution from hydroxyl (O-H, E_b ~ 531.5 eV) (**Fig. 2c**)[29-31]. As the hydrogen spillover progressed, the deconvoluted O-V peak gradually decreased and O-H peak increased, which denotes a substantial increase of hydroxyl bonding by reversible hydrogen incorporation from Pt catalyst into the lattice. More interestingly, during hydrogen spillover under the reaction of Pt/VO_2 with H_2 gas, a non-negligible shoulder peak appeared at the highest binding energy of 532.6 eV; this peak could not be detected in *ex situ* X-ray photoemission spectroscopy measured under vacuum[10] (**Fig. 2c**). This shoulder peak could be assigned to adsorbed water molecules (H_2O) on the VO_2 thin film surface [29, 32, 33]; this additional peak provides strong evidence that weakly-adsorbed water molecules, as well as hydroxyl bonded to the lattice, form on the film surface when hydrogen gas reacts with the surface of VO_2 during hydrogen spillover.

Real-time surface characterization was repeated using APXPS at 30 °C while introducing hydrogen gas. Peak shift and broadening of V $2p_{3/2}$ at 517 eV and O 1s at 530 eV occurred in the same direction as at 50 °C, but at a significantly-diminished rate (**Fig. S2**). The difference indicates that temperature strongly affects the surface reaction on the VO_2 by hydrogen spillover. Detailed deconvolution of APXPS spectra at 30 °C showed a decrease of V^{5+} in V $2p_{3/2}$ signal, and an increase in hydroxyl groups (O-H) in O 1s, but no shoulder peak by adsorbed water

molecules; this result indicates that the formation of water during hydrogen spillover requires sufficient thermal energy to overcome an activation barrier.

To quantify the real-time change in the valence states of vanadium ions at the surface of VO_2 during hydrogen spillover, the areas A of each deconvoluted peak ($V^{3+¿2p_{3/2}¿}$, $V^{4+¿2p_{3/2}¿}$, $V^{5+¿2p_{3/2}¿}$) were calculated, then normalized by the total area of $V\,2p_{3/2}$ (**Figs. 3a, b**). The normalized area indirectly indicates the relative ratio of each valence state (¿) as a function of hydrogen spillover duration t as[34]

¿¿, (1)

where $A¿$ is the area under the deconvoluted peaks of V^{n+} ($n \in$ [35]) at time t, and $A(V\,2p_{3/2}, t)$ is the total area of $V\,2p_{3/2}$ at time t. As expected, the contributions of valence states decreased from V^{5+} to V^{4+} to V^{3+} during hydrogen spillover (**Figs. 3a, b**). Therefore, conversions from V^{5+} to V^{4+} and from V^{4+} to V^{3+} occurred concurrently due to the electron supply induced by hydrogen uptake. This reduction rate was faster at 50 °C than at 30 °C; the difference confirms that the surface reaction for hydrogen spillover does not occur until sufficient activation energy is provided (**Fig. 3c**).

In the same fashion, the oxygen contents near the surfaces were characterized quantitatively in real time by normalizing each deconvoluted peaks in O 1s spectra. The area under an O 1s spectrum normalized by that of V $2p_{3/2}$ is a quantitative measure of the oxygen content relative to vanadium atoms near the surface (i.e., $[O]$ at $<$ 1 nm); therefore, to monitor the

kinetic changes over time, the normalized area of an O 1s spectrum was quantified using those peaks as[34]

$$[O](t) = A(O\,1s,t)_{norm} = \frac{A(O\,1s,t)/A(V\,2p_{3/2},t)}{A(O\,1s,0)/A(V\,2p_{3/2},¿0)¿}, \quad (2)$$

where $A(O\,1s,t)$ and $A(O\,1s,0)$ are the area of total 1s spectra at times t and 0, respectively. During hydrogen spillover, $[O]$ gradually decreased to ~ 10.34% at 50 °C and ~ 5.42 % at 30 °C (**Fig. 3d**); these changes indicate a loss of surface lattice oxygen during hydrogen spillover, and suggest that the hydrogen spillover process involves release of oxygen at the surface. The loss of surface lattice oxygen was unexpected, and indicates that oxygen deficiencies are likely to occur at the VO_2 surface, unlike hydrogen incorporation in the VO_2 bulk lattice even during hydrogen spillover at low temperature. Despite the topotactic phase transformation in VO_2 bulk lattice during hydrogen spillover, oxygen at the surface cannot be preserved during hydrogen spillover; surface oxygen vacancies, as well as hydrogen interstitials, are responsible for the reduction of vanadium valence states.

To further elucidate the origin of oxygen loss, the O 1s signals were classified by the area of each deconvoluted peak (O-V, O-H, H_2O-related peaks) and each contribution from the O 1s signals was plotted as a function of spillover time (**Fig. 3e, 3f**). The amount of oxygen related to each deconvoluted O 1s peaks can be estimated as

$$[O-V](t) = A(O-V\,1s,t)_{norm} = \frac{A(O-V\,1s,t)/A(V\,2p_{3/2},t)}{A(O-V\,1s,0)/A(V\,2p_{3/2},¿0)¿}. \quad (3)$$

$$[O-H](t)=A(O-V\,1s,t)_{norm}=\frac{A(O-H\,1s,t)/A(V\,2p_{3/2},t)}{A(O-H\,1s,0)/A(V\,2p_{3/2},¿0)¿}. \quad (4)$$

$$[H_2O](t)=A(H_2O\,1s,t)_{norm}=\frac{A(H_2O\,1s,t)/A(V\,2p_{3/2},t)}{A(H_2O\,1s,0)/A(V\,2p_{3/2},¿0)¿}. \quad (5)$$

where $[O-V]$, $[O-H]$, $[H_2O]$ are the amounts of oxygen related to lattice oxygen, hydroxyl, and weakly adsorbed H_2O at the surface, respectively. As hydrogen spillover proceeded, $[O-V]$ decreased and $[O-H]$ and $[H_2O]$ increased at 50 °C, but only $[O-H]$ increased at 30 °C. The formation of weakly-adsorbed H_2O depends more strongly on the temperature than the formation of hydroxyl does. Weakly-adsorbed H_2O is not chemically bonded to the lattice of VO_2 surface, so the oxygen in the lattice is regarded as the sum of $[O-V]$ and $[O-H]$. Thus, estimated actual loss of surface lattice oxygen was as much as ~ 25 % at 50 °C. Remarkably, the increase of $[H_2O]$ coincides with the oxygen loss in the lattice; this relationship indicates that the formation of weakly-adsorbed H_2O from the lattice may be related to the oxygen loss in the lattice at the surface.

First-principles density functional theory (DFT) calculations were employed to investigate the possibility that H_2O forms and oxygen is lost from the surface of VO_2 during hydrogen spillover. For the study, we constructed the most energetically stable (110) surface structure of rutile VO_2.[25] The simulation considered 12 atomic layers (~ 19.63 Å) along the thickness direction; the bottom three layers were fixed to represent bulk layers, so nine atomic layers were allowed to be fully relaxed at the surface. We compared the energetic stability of possible adsorption structures when two hydrogens were added to the fully oxidized VO_2 surface. **Fig. 4a-d** shows the schematic view of four different configurations of two hydrogen adatoms at

on the VO_2 surface: H_2 physisorption (**Fig. 4a**), two sub-surface interstitials ($2H_i$) (**Fig. 4b**), two hydrogens binding with one oxygen to form a water molecule (H_2O) (**Fig. 4c**), and two hydrogens binding with an oxygen to form two hydroxyl groups (2OH) at the surface (**Fig.4d**); these configurations have distinct thermodynamic adsorption energies (**Fig. 4e**). The DFT calculation predicted that before hydrogen spillover, H_2 physisorption on VO_2 surface (i.e., the states) has very small thermodynamic adsorption energy (0.07 eV). In contrast, three chemisorbed configurations are energetically stable; the predicted adsorption energies are 0.99 eV for $2H_i$, 2.28 eV for H_2O, and 1.80 eV for 2OH. Thus, the H_2 molecule is likely to be incorporated on VO_2 surface by dissociative chemisorption after the activation barriers are overcome by the Pt catalyst during spillover. More importantly, the formation of H_2O molecule is energetically the most favorable among the different chemisorption configurations; this result is consistent with our APXPS observation during hydrogenation.

We also simulated the variation of bonding energy of a surface oxygen atom when one or two hydrogens was chemisorbed on it. Our DFT calculation predicts that the bonding energy of the surface oxygen decreased from 4.14 eV to 3.51 eV when it absorbed one hydrogen atom, and to 0.84 eV when it absorbed two hydrogen atoms. Thus, the absorbed hydrogen atoms weaken the binding between the surface oxygen atom and the VO_2 surface. This calculation supports our experimental observation that the two adsorbed or interstitial hydrogens tend to interact with a surface oxygen atom on VO_2 surfaces by forming a H_2O molecule with hydrogen bonding above the VO_2 surface, and thereby leaving oxygen vacancies at the surface.

As the Pt catalyst lowers the activation barrier for surface reaction and the hydrogen spillover ($H_2 \xrightarrow{Pt} 2H$) proceeds at low temperature, the dissociated hydrogen first spreads gradually to the surface of the support. The hydrogen atoms lose their electron when they coordinate to oxygen, and this change causes a reduction of valence states on the transition metal adjacent to the absorption sites: the hydrogen atoms react with lattice oxygen on the surface ($O^x_{O(S)}$) to form positively charged hydroxyl $(OH)_{O(S)}$ at the terminal oxygen and electrons $e^{-¿¿}$ on the VO_2 surface near the dispersed Pt as described in Kroger-Vink notation[6, 33, 36]:

$$2H + 2O^x_{O(S)} \rightarrow 2(OH)_{O(S)} + 2e^{-¿¿}. \quad (6)$$

In the bulk, the hydrogen ions from the hydroxyl bonds at the surface are likely to diffuse into the bulk VO_2 without losing oxygen (i.e., bulk diffusion)[36]. Hydrogen ions from the surface migrate along a facile diffusion pathway by hydrogen transfer between oxygen atoms through the interstitial sites of VO_2[13], which can be detected by SIMS. The calculated activation barriers for hydrogen migration were 0.4 eV, which is low enough that interstitial hydrogen can move even at low temperature. Electrons supplied by ionization of hydrogen atoms simultaneously reduce the valence states of vanadium ($V^{5+} \rightarrow V^{4+} \rightarrow V^{3+}$). Thus, hydrogen diffusion by interstitial site in VO_2 bulk ($2H_{i(B)}$) can be described as

$$2(OH)_{O(S)} \rightarrow 2O^x_{O(S)} + 2H_{i(B)}. \quad (7)$$

However, as a competing reaction at the surface, two hydrogen atoms are likely to combine with a lattice oxygen to form water (H_2O); these hydrogens do not diffuse back into the bulk, but they are likely to take the surface oxygen out of the surface ($V_{O(S)}$), as probed by

APXPS. Since electrons are also supplied to meet charge neutrality in the lattice, this reaction at the surface also reduces the valence states of vanadium by supplying electrons:

$$2(OH)_{O(S)} \rightarrow H_2O(l) + O^{x}_{O(S)} + V_{O(S)} \qquad (8)$$

Reaction (8) runs in exactly the opposite direction to the effects of steam treatment on the dispersed Pt/oxide support catalyst[37, 38]: Under steam-treatment condition, water molecules can fill the oxygen vacancies on dispersed Pt/CeO_2 surfaces, and thereby generate two active hydroxyls near the Pt.[37] The simultaneous detection of the evidence for oxygen loss from the lattice and the formation of water by APXPS during hydrogen spillover strongly support the hypothesis that reaction (8) occurs at the surface. Unlike dominant reaction of the formation of hydrogen interstitials in the bulk VO_2, both oxygen vacancies and hydrogen interstitials coexist due to the two competing reactions at the surface. Under reducing conditions, the bridging vacancies near the surface are likely to form more easily than the vacancies in the bulk beneath the surface; this conclusion is consistent with previous reports on the tendency of oxygen vacancies near the surface of rutile TiO_2.[25, 39] Our observation infers that dominant defects (oxygen vacancies vs. hydrogen interstitial) can be delicately changeable depending on the degree of lattice coordination under reducing condition, and thus could extend this principle to the recent controversial debates on ionic-defect-induced phase transition in the channel of VO_2 by ionic liquid gating.[40, 41]

In summary, we have elucidated the mechanism that modulates the surface chemistry of VO_2 epitaxial films during the process of hydrogen spillover. Quantitative analysis using *in-situ* APXPS combined with DFT results indicated that numerous surface oxygen vacancies form

during the hydrogen-spillover process; this conclusion contradicts the general belief that formation of hydrogen interstitials is the dominant process without the loss of oxygens in the entire VO_2 films. The facile formation of oxygen vacancies is attributed into the fact that surface reaction generates weakly-adsorbed water from the less coordinated surface atoms, and that the resulting water molecules bind less strongly than the hydrogen that diffuses into the bulk during hydrogen spillover. These real-time observations provide new insight about surface reaction and defect formation in correlated oxides during catalytic reaction.

Supporting Information

Supporting Information is available free of charge on the ACS publications website.

Acknowledgements

We acknowledge support for this work by the Basic Science Research Program (2017R1A2B2007819, 2017M2A2A6A01020116, 2017K1A3A7A09040044) through the National Research Foundation of Korea (NRF) funded by the Ministry of Science and ICT, and by Ministry of Trade, Industry and Energy (10076608).

Author contributions

J. S., K. I. and H. Y. conceived the idea and designed the study; H. Y. performed the film growth and synchrotron in-situ x-ray diffraction and SIMS measurement; H. Y., Y. K., J. S. and K. I. performed APXPS measurement with the assistance of E. J. C.; H. Y. analyzed the APXPS data under the supervision of K. I. and J. S.; D. L. performed first-principles calculation; J. S. and H. Y. wrote the manuscript and all authors commented on it.

Conflicts of interest

The authors have no competing financial interest.

References

1. Prins, R., Hydrogen spillover. Facts and fiction. *Chem. Rev.* **2012,** *112* (5), 2714-2738.

2. Marcinkowski, M. D.; Jewell, A. D.; Stamatakis, M.; Boucher, M. B.; Lewis, E. A.; Murphy, C. J.; Kyriakou, G.; Sykes, E. C. H., Controlling a spillover pathway with the molecular cork effect. *Nature Mater.* **2013,** *12* (6), 523.

3. Im, J.; Shin, H.; Jang, H.; Kim, H.; Choi, M., Maximizing the catalytic function of hydrogen spillover in platinum-encapsulated aluminosilicates with controlled nanostructures. *Nature Commun.* **2014,** *5*, 3370.

4. Karim, W.; Spreafico, C.; Kleibert, A.; Gobrecht, J.; VandeVondele, J.; Ekinci, Y.; van Bokhoven, J. A., Catalyst support effects on hydrogen spillover. *Nature* **2017,** *541* (7635), 68.

5. Khoobiar, S., Particle to particle migration of hydrogen atoms on platinum—alumina catalysts from particle to neighboring particles. *J. Phys. Chem.* **1964,** *68* (2), 411-412.

6. Chen, L.; Cooper, A. C.; Pez, G. P.; Cheng, H., On the mechanisms of hydrogen spillover in MoO3. *J. Phys. Chem. C* **2008,** *112* (6), 1755-1758.

7. Zhou, Y.; Guan, X. F.; Zhou, H.; Ramadoss, K.; Adam, S.; Liu, H. J.; Lee, S.; Shi, J.; Tsuchiya, M.; Fong, D. D.; Ramanathan, S., Strongly correlated perovskite fuel cells. *Nature* **2016,** *534* (7606), 231-234.

8. Panayotov, D. A.; Yates, J. T., Spectroscopic detection of hydrogen atom spillover from au nanoparticles supported on TiO2: Use of conduction band electrons. *J. Phys. Chem. C* **2007,** *111* (7), 2959-2964.

9. Park, J.; Yoon, H.; Choi, S.-Y.; Son, J., Nanoscaffold WO3 by Kinetically Controlled

Polymorphism. *Cryst. Growth Des.* **2018,** *19* (1), 479-486.

10. Yoon, H.; Choi, M.; Lim, T.-W.; Kwon, H.; Ihm, K.; Kim, J. K.; Choi, S.-Y.; Son, J., Reversible phase modulation and hydrogen storage in multivalent VO2 epitaxial thin films. *Nature Mater.* **2016,** *15* (10), 1113-1119.

11. Shi, J.; Zhou, Y.; Ramanathan, S., Colossal resistance switching and band gap modulation in a perovskite nickelate by electron doping. *Nature Commun.* **2014,** *5*, 4860.

12. Oh, C.; Heo, S.; Jang, H. M.; Son, J., Correlated memory resistor in epitaxial NdNiO3 heterostructures with asymmetrical proton concentration. *Appl. Phys. Lett.* **2016,** *108* (12), 122106.

13. Yoon, H.; Park, J.; Choi, S. Y.; Lee, D.; Son, J., Facet-Dependent Phase Control by Band Filling and Anisotropic Electron–Lattice Coupling in HVO2 Epitaxial Films. *Adv. Electron. Mater.* **2018,** *4*, 1800128.

14. Wei, J.; Ji, H.; Guo, W. H.; Nevidomskyy, A. H.; Natelson, D., Hydrogen stabilization of metallic vanadium dioxide in single-crystal nanobeams. *Nature Nanotech.* **2012,** *7* (6), 357-362.

15. Filinchuk, Y.; Tumanov, N. A.; Ban, V.; Ji, H.; Wei, J.; Swift, M. W.; Nevidomskyy, A. H.; Natelson, D., In Situ Diffraction Study of Catalytic Hydrogenation of VO2: Stable Phases and Origins of Metallicity. *J Am Chem Soc* **2014,** *136* (22), 8100-8109.

16. Chen, J. K.; Mao, W.; Ge, B. H.; Wang, J.; Ke, X. Y.; Wang, V.; Wang, Y. P.; Dobeli, M.; Geng, W. T.; Matsuzaki, H.; Shi, J.; Jiang, Y., Revealing the role of lattice distortions in the hydrogen-induced metal-insulator transition of SmNiO3. *Nature Commun.* **2019,** *10*, 694.

17. Jeen, H.; Choi, W. S.; Biegalski, M. D.; Folkman, C. M.; Tung, I. C.; Fong, D. D.;

Freeland, J. W.; Shin, D.; Ohta, H.; Chisholm, M. F.; Lee, H. N., Reversible redox reactions in an epitaxially stabilized SrCoOx oxygen sponge. *Nature Mater.* **2013,** *12* (11), 1057-1063.

18. Hu, S.; Seidel, J., Oxygen content modulation by nanoscale chemical and electrical patterning in epitaxial SrCoO3-delta (0 < delta <= 0.5) thin films. *Nanotechnology* **2016,** *27* (32), 325301.

19. Zhao, Y.; Karaoglan-Bebek, G.; Pan, X.; Holtz, M.; Bernussi, A. A.; Fan, Z., Hydrogen-doping stabilized metallic VO2 (R) thin films and their application to suppress Fabry-Perot resonances in the terahertz regime. *Appl. Phys. Lett.* **2014,** *104* (24), 241901.

20. Chen, Y. L.; Wang, Z. W.; Chen, S.; Ren, H.; Wang, L. X.; Zhang, G. B.; Lu, Y. L.; Jiang, J.; Zou, C. W.; Luo, Y., Non-catalytic hydrogenation of VO2 in acid solution. *Nature Commun.* **2018,** *9*, 818.

21. Stoerzinger, K. A.; Hong, W. T.; Crumlin, E. J.; Bluhm, H.; Biegalski, M. D.; Shao-Horn, Y., Water Reactivity on the LaCoO3 (001) Surface: An Ambient Pressure X-ray Photoelectron Spectroscopy Study. *J. Phys. Chem. C* **2014,** *118* (34), 19733-19741.

22. Lu, Q. Y.; Chen, Y.; Bluhm, H.; Yildiz, B., Electronic Structure Evolution of SrCoOx during Electrochemically Driven Phase Transition Probed by in Situ X-ray Spectroscopy. *J. Phys. Chem. C* **2016,** *120* (42), 24148-24157.

23. Manning, T. D.; Parkin, I. P.; Pemble, M. E.; Sheel, D.; Vernardou, D., Intelligent window coatings: Atmospheric pressure chemical vapor deposition of tungsten-doped vanadium dioxide. *Chem Mater* **2004,** *16* (4), 744-749.

24. Kim, G.; Yoon, J.; Yang, H.; Lim, H.; Lee, H.; Jeong, C.; Yun, H.; Jeong, B.; Crumlin, E.; Lee, J.; Lee, J.; Ju, H.; Mun, B. S., Observation of in situ oxidation dynamics of

vanadium thin film with ambient pressure X-ray photoemission spectroscopy. *J Appl Phys* **2016,** *120* (20), 205305.

25. Mellan, T. A.; Grau-Crespo, R., Density functional theory study of rutile VO2 surfaces. *J. Chem. Phys.* **2012,** *137* (15), 154706.

26. Seah, M. P.; Dench, W., Quantitative electron spectroscopy of surfaces: A standard data base for electron inelastic mean free paths in solids. *Surf. Interface Anal.* **1979,** *1* (1), 2-11.

27. Stoerzinger, K. A.; Hong, W. T.; Crumlin, E. J.; Bluhm, H.; Shao-Horn, Y., Insights into Electrochemical Reactions from Ambient Pressure Photoelectron Spectroscopy. *Accounts Chem Res* **2015,** *48* (11), 2976-2983.

28. Stoerzinger, K. A.; Favaro, M.; Ross, P. N.; Yano, J.; Liu, Z.; Hussain, Z.; Crumlin, E. J., Probing the Surface of Platinum during the Hydrogen Evolution Reaction in Alkaline Electrolyte. *J Phys Chem B* **2018,** *122* (2), 864-870.

29. Silversmit, G.; Depla, D.; Poelman, H.; Marin, G. B.; De Gryse, R., Determination of the V2p XPS binding energies for different vanadium oxidation states (V5+ to V0+). *J Electron Spectrosc* **2004,** *135* (2-3), 167-175.

30. Kačiulis, S.; Mattogno, G.; Napoli, A.; Bemporad, E.; Ferrari, F.; Montenero, A.; Gnappi, G., Surface analysis of biocompatible coatings on titanium. *J Electron Spectrosc* **1998,** *95* (1), 61-69.

31. Philippin, G.; Delhalle, J.; Mekhalif, Z., Comparative study of the monolayers of CH3 (CH2) n SiCl3 and CH3 (CH2) n PO (OH) 2, n= 4 and 13, adsorbed on polycrystalline titanium substrates. *Appl. Surf. Sci.* **2003,** *212*, 530-536.

32. Dupin, J.-C.; Gonbeau, D.; Vinatier, P.; Levasseur, A., Systematic XPS studies of metal

oxides, hydroxides and peroxides. *Phys. Chem. Chem. Phys.* **2000,** *2* (6), 1319-1324.

33. Mun, B. S.; Liu, Z.; Motin, M. A.; Roy, P. C.; Kim, C. M., In situ observation of H2 dissociation on the ZnO (0001) surface under high pressure of hydrogen using ambient-pressure XPS. *Int. J. Hydrog. Energy* **2018,** *43* (18), 8655-8661.

34. Gopal, C. B.; Garcia-Melchor, M.; Lee, S. C.; Shi, Y. Z.; Shavorskiy, A.; Monti, M.; Guan, Z. X.; Sinclair, R.; Bluhm, H.; Vojvodic, A.; Chueh, W. C., Equilibrium oxygen storage capacity of ultrathin CeO2-delta depends non-monotonically on large biaxial strain. *Nature Commun.* **2017,** *8*, 15360.

35. Blöchl, P. E., Projector augmented-wave method. *Phys. Rev. B* **1994,** *50* (24), 17953.

36. Warnick, K. H.; Wang, B.; Pantelides, S. T., Hydrogen dynamics and metallic phase stabilization in VO2. *Appl. Phys. Lett.* **2014,** *104* (10), 101913.

37. Nie, L.; Mei, D. H.; Xiong, H. F.; Peng, B.; Ren, Z. B.; Hernandez, X. I. P.; DeLariva, A.; Wang, M.; Engelhard, M. H.; Kovarik, L.; Datye, A. K.; Wang, Y., Activation of surface lattice oxygen in single-atom Pt/Ce0(2) for low-temperature CO oxidation. *Science* **2017,** *358* (6369), 1419-1423.

38. Ketteler, G.; Yamamoto, S.; Bluhm, H.; Andersson, K.; Starr, D. E.; Ogletree, D. F.; Ogasawara, H.; Nilsson, A.; Salmeron, M., The nature of water nucleation sites on TiO2(110) surfaces revealed by ambient pressure X-ray photoelectron spectroscopy. *J. Phys. Chem. C* **2007,** *111* (23), 8278-8282.

39. Vijay, A.; Mills, G.; Metiu, H., Adsorption of gold on stoichiometric and reduced rutile TiO2 (110) surfaces. *J. Chem. Phys.* **2003,** *118* (14), 6536-6551.

40. Jeong, J.; Aetukuri, N.; Graf, T.; Schladt, T. D.; Samant, M. G.; Parkin, S. S. P.,

Suppression of Metal-Insulator Transition in VO2 by Electric Field-Induced Oxygen Vacancy Formation. *Science* **2013,** *339* (6126), 1402-1405.

41. Ji, H.; Wei, J.; Natelson, D., Modulation of the Electrical Properties of VO2 Nanobeams Using an Ionic Liquid as a Gating Medium. *Nano Lett.* **2012,** *12* (6), 2988-2992.

Figure Captions

Figure 1 | (**a**) Schematic illustration of *in situ* XRD and APXPS measurement during hydrogen spillover on VO_2 surface with Pt islands, which had been formed on the VO_2 surface as a H_2 dissociation catalyst. (**b**) *In situ* symmetrical XRD line plot and intensity map of 10-nm-thick epitaxial VO_2 thin film on (0001) Al_2O_3 during hydrogenation at 70 °C. The out-of-plane lattice was hugely expanded by massive hydrogen incorporation in the bulk of VO_2 films. TOF-SIMS negative ion depth profiles of (**c**) pristine VO_2 film and (**d**) hydrogenated VO_2 film on (0001) Al_2O_3 after the hydrogen spillover for 8 h at 50 °C. Hydrogens were selectively incorporated in the entire VO_2 film, but loss of oxygen was negligible.

Figure 2 | *In-situ* APXPS spectra of VO_2 epitaxial films on (0001) Al_2O_3 during hydrogen spillover (H_2 pressure 5 mTorr) at 50 °C using 670-eV photon energy with inelastic mean free paths of ~ 1.2 nm. Intensity map of (**a**) V $2p_{3/2}$ and (**b**) O 1s core-level as a function of time. During hydrogen spillover, the vanadium core level shifted to lower binding energy as the oxygen core level shifted to higher binding energy. (**c**) *In-situ* APXPS evolution of V 2p and O 1s photoelectron peak with peak deconvolution. V 2p peaks were deconvoluted to V^{3+}, V^{4+} and V^{5+}; O 1s peaks were deconvoluted to lattice oxygen (O-V), hydroxyl (O-H), and adsorbed water (H_2O).

Figure 3 | The relative ratio of each vanadium valence state ($[V^{n+}]$) as a function of hydrogen

spillover duration at (**a**) 50 °C and (**b**) 30 °C. The vanadium valence states decreased from V^{5+} and V^{4+} to V^{3+} during hydrogen spillover; this trend indicate that valences state were reduced. (**c**) Fraction of integrated [V^{3+}] peak area as a function of time at different temperature (50 °C, 30 °C). (**d**) Fraction of integrated [O] peak area as a function of time at different temperature (50 °C, 30 °C). Note that $[O]$ gradually decreased down to ~ 10.34% (at 50 °C) and ~ 5.42 % (at 30 °C) by proceeding hydrogen spillover, which indicates the loss of surface lattice oxygen during hydrogen spillover. The relative ratio of each deconvoluted peaks in O 1s spectra (O-V, O-H, H_2O-related peaks) as a function of hydrogen spillover duration at (**e**) 50 °C and (**f**) 30 °C. Weakly-adsorbed H_2O does not bind chemically to the lattice of VO_2 surfaces, so actual loss of surface lattice oxygen can be estimated to be up to ~ 25.24 % at 50 °C.

Figure 4 | Schematic view of predicted four different adsorption configurations of H_2 at VO_2 surface using first principles calculations: (**a**) H_2 (**b**) $2H_i$ (**c**) H_2O (**d**) 2OH. (**e**) Comparison of calculated adsorption energies of four different configurations. The formation of H_2O molecule is energetically the most favorable among the different chemisorption configurations at the surface.

Figure 1

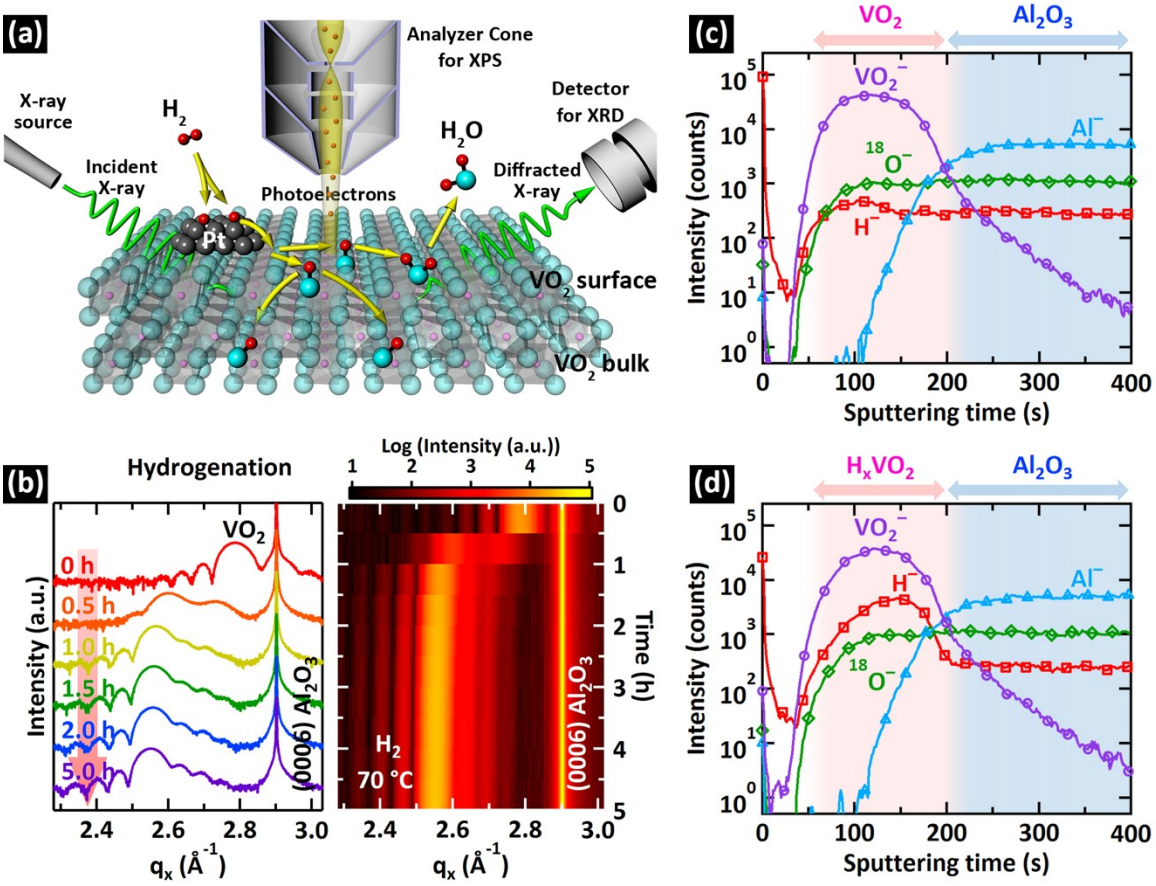
(a)
Analyzer Cone for XPS
X-ray source
H2
Incident X-ray
Photoelectrons
H2O
Detector for XRD
Diffracted X-ray
Pt
VO2 surface
VO2 bulk
(b)
Hydrogenation
Log (Intensity (a.u.))
VO2
0 h
0.5 h
1.0 h
1.5 h
2.0 h
5.0 h
Intensity (a.u.)
(0006) Al2O3
H2
70 °C
Time (h)
qx (Å-1)
(c)
VO2
Al2O3
VO2−
Al−
18O−
H−
Intensity (counts)
Sputtering time (s)
(d)
HxVO2
Al2O3
VO2−
H−
Al−
18O−
Intensity (counts)
Sputtering time (s)

Figure 2

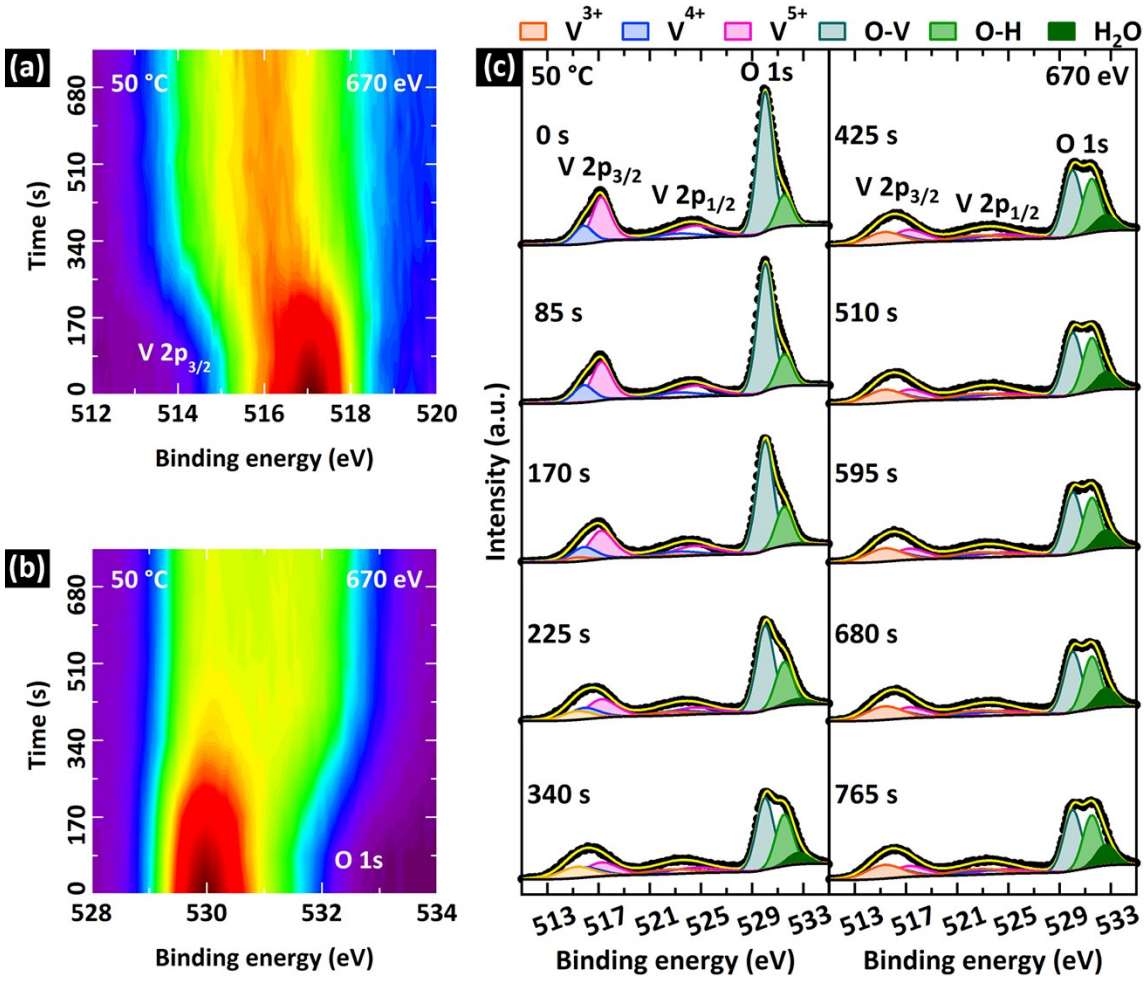
(a)
50 °C
670 eV
V 2p3/2
Time (s)
0
170
340
510
680
512
514
516
518
520
Binding energy (eV)
(b)
50 °C
670 eV
O 1s
Time (s)
0
170
340
510
680
528
530
532
534
Binding energy (eV)
(c)
V3+
V4+
V5+
O-V
O-H
H2O
50 °C
O 1s
0 s
V 2p3/2
V 2p1/2
85 s
170 s
225 s
340 s
670 eV
425 s
O 1s
V 2p3/2
V 2p1/2
510 s
595 s
680 s
765 s
Intensity (a.u.)
513 517 521 525 529 533
Binding energy (eV)
513 517 521 525 529 533
Binding energy (eV)

Figure 3

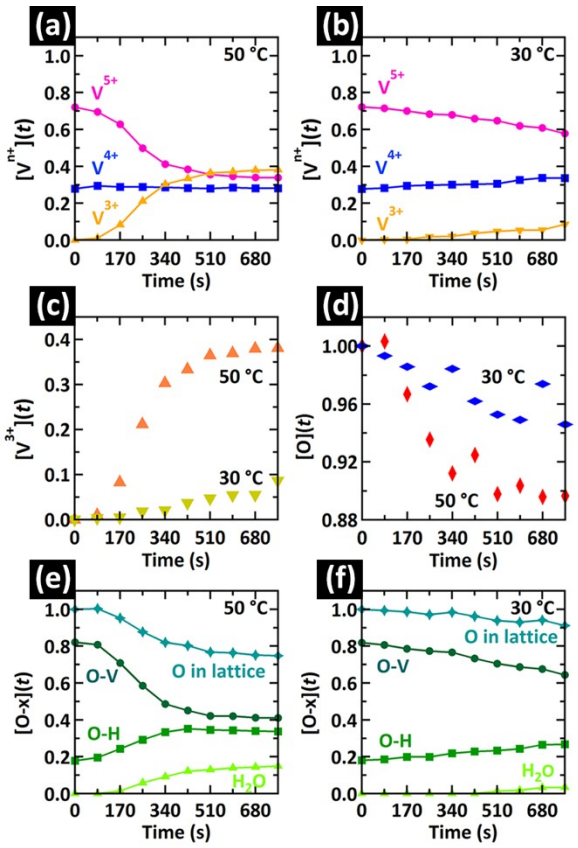
(a)
50 °C
V5+
V4+
V3+
[Vn+](t)
Time (s)
(b)
30 °C
(c)
50 °C
30 °C
[V3+](t)
(d)
30 °C
50 °C
[O](t)
(e)
50 °C
O-V
O in lattice
O-H
H2O
[O-x](t)
(f)
30 °C
O in lattice
O-V
O-H
H2O

Figure 4